Sensors and Materials, Vol. 37, No. 4 (2025) 1537–1550
MYU Tokyo

S & M 4003

Measurement Circuit Design of 3-in-1 Microsensor Embedded in Proton Exchange Membrane Water Electrolyzer

Chi-Yuan Lee,[1] Zhi-Yu Huang,[1] Jia-Yu Hsu,[1] Ting-Fu Kuo,[2] and Zhi-Xuan Dai[2*]

[1]Department of Mechanical Engineering, Yuan Ze Fuel Cell Center, Yuan Ze University,
No. 135, Yuandong Rd., Zhongli Dist., Taoyuan City 320315, Taiwan (R.O.C.)
[2]Department of Bio-Industrial Mechatronics Engineering, National Chung Hsing University,
No. 145, Xingda Rd., South Dist., Taichung City 402202, Taiwan (R.O.C.)

(Received May 13, 2024; accepted August 22, 2024)

Keywords: PEMWE, microsensor, real-time microscopic monitoring

The proton exchange membrane water electrolyzer (PEMWE) has the advantages of simplicity, small size, high current density, and high operating temperature, but it is easy to cause corrosion and oxidation to the gas diffusion layer or electrode at the oxygen end during electrolysis, which will accelerate the degradation of its performance. Therefore, a flexible 3-in-1 microsensor (temperature, voltage, and current) was developed using MEMS technology and embedded inside the PEMWE used in this study, and the circuit was designed and the data was observed in real time by Arduino Mega 2560. When the PEMWE is running, a flexible 3-in-1 microsensor can predict the performance in advance and obtain valuable information about the aging or failure of the PEMWE, so that it can be warned and adjusted in time.

1. Introduction

To date, a considerable amount of research has been conducted to address issues of greenhouse gas emissions and air pollution resulting from the combustion of fossil fuels.(1–3) Proton exchange membrane fuel cells (PEMFCs) are considered a promising energy source for meeting future transportation needs owing to their low operating temperature and high energy efficiency.(4–6) Achieving net-zero carbon emissions has become a global imperative. As of September 2021, 55 countries have committed to national net-zero emission targets.(7) The limited reserves of fossil fuels and their adverse environmental impacts necessitate the urgent task of finding an abundant, renewable, recyclable, clean, and safe source of fuel.(8) If renewable energy is used for water electrolysis to produce hydrogen, it can result in low-carbon green hydrogen. Water electrolysis is an effective technology for reducing carbon emissions, and proton exchange membrane water electrolyzers (PEMWEs) offer advantages such as simplicity, small size, high current density, and high operating temperature. Hydrogen, as an attractive alternative energy carrier, demonstrates significant potential in mitigating global overreliance on non-renewable resources owing to its high energy density (140 MJ kg^{-1}) and environmentally friendly characteristics.(9,10) However, up to now, most of the hydrogen has been produced under

---

[*]Corresponding author: e-mail: zxdai@nchu.edu.tw
https://doi.org/10.18494/SAM5139

ISSN 0914-4935
https://myukk.org/

stringent conditions through the steam methane reforming of natural gas or other fossil fuels,(11,12) and the conversion efficiency is energy-intensive, often accompanied by the release of unfavorable carbon dioxide byproducts.(13,14) Therefore, exploring high-efficiency green hydrogen production technologies is a crucial pathway to reducing carbon emissions and achieving carbon neutrality.(15)

The minimum electrical energy required for a battery decreases with an increase in temperature.(16) Therefore, raising the operating temperature of the PEMWE system can enhance performance and power efficiency. However, membrane stability begins to decrease at temperatures above 100 °C, so ideally, the operating temperature is limited to the range of 70–90 °C. It may be even lower when processing aids are added to the water. Hence, monitoring and controlling the temperature of the PEMWE system are crucial. Therefore, in this study, we chose to observe the performance of the PEMWE by monitoring three data points: temperature, voltage, and current. A flexible three-in-one microsensor (temperature, voltage, and current) was developed using MEMS technology for the real-time monitoring of these three physical quantities. The current measurement serves as an indicator of performance, while the temperature observation helps prevent a decrease in membrane stability. Ogumerem and Pistikopoulos measured the temperature and pressure at the inlet and outlet of the PEMWE externally and applied real-time data control to regulate temperature, reducing the rate of membrane degradation.(17) When the outlet temperature remained lower than the inlet temperature and the ambient temperature was below the outlet temperature (295 K), the controller was activated at the beginning of the experiment. It is evident that real-time predictions through machine learning contribute to immediate parameter control. If the flexible microsensor developed in our laboratory is employed to measure internal data and make predictions in real time, it would yield more accurate results.

Electrolysis is a natural choice and has the potential to significantly impact the long-term sustainable integration of variable renewable energy resource into the energy landscape.(18–22) If integrated with a fuel cell, the hydrogen and oxygen produced from electrolysis are used in a reverse process to generate electricity when other sources are not able to meet the electricity demand.(23,24) PEM water electrolysis is the most promising type of electrolysis owing to its higher current density and gas purity. PEM water electrolysis also has a compact design and flexible operation. The flexibility of the PEMWE makes it very suitable for integration with variable renewable energy as an energy storage path.(23)

In previous experiments, our laboratory often used the NI PXI 2575 data collector for data collection.(25,26) This machine can directly and accurately read voltage, current, and resistance values without circuit design. Although the experimental data obtained using the NI PXI 2575 data collector has a higher accuracy than most commercial development boards (such as Arduino and Raspberry Pi), its real-time data reading capability is limited by the system. It can only analyze and judge the entire data set after the experiment, which limits future development that requires real-time signal reading. Therefore, a circuit was designed to convert the current and resistance values into voltage signals for the development board to read. In the future, these data can be utilized through machine learning to build a performance prediction model using Python. Subsequently, this prediction model can be installed on a Raspberry Pi, enabling it to predict performance in real time while the water electrolyzer is operating. This allows for the early prediction of valuable information regarding aging or failure within the PEMWE. With this advance warning, timely adjustments can be made, resulting in a more stable hydrogen production efficiency.

The PEMWE is the most advanced type of water electrolyzer and holds the potential to be the most efficient, environmentally friendly, and cost-effective electrochemical device for hydrogen production when compared with other conventional electrolyzers and hydrocarbon steam reformers.(27) Hydrogen production through water electrolysis involves considerations of both power sources and electrolysis efficiency. To reduce energy consumption and enhance production, the PEMWE was developed in response to these challenges. The first PEMWE was manufactured by General Electric in 1966 for space technology applications. Compared with traditional water electrolysis techniques, the PEMWE offers advantages such as high energy efficiency and low operating temperature.(28) The main components of a high-pressure PEMWE include end plates, current collectors, channels, and the membrane electrode assembly (MEA).(29) In the internal cell of a high-pressure PEMWE, water is delivered to the anode channel, diffuses through the porous electrode, and electrolysis reactions occur at the interface of the anode membrane. Excess water is transported into the cell to remove the heat generated by irreversible reactions and ensure the concentration of reactants on the surface of the active electrode. The anode inlet and outlet consist of water and oxygen, while water flow is introduced to the cathode to enhance hydrogen discharge and prevent membrane drying. The cathode produces water and hydrogen, particularly under high-pressure operating conditions, facilitating the transfer of water to the other side of electrolysis.(29) Compared with atmospheric-pressure water electrolyzers, high-pressure water electrolyzers exhibit high hydrogen production efficiency.

A previous laboratory has published similar articles.(30) The major difference with theirs lies in the use of a circuit design for data extraction in this study, coupled with double confirmation. The advantage is that if commercialized later, it can significantly reduce costs.

2. Three-in-one Microsensor Manufacturing Process

2.1 Design of flexible three-in-one microsensor

To achieve mass production for cost reduction, the three-in-one microsensor (temperature, voltage, and current) used in this study has reduced the size of the sensing head compared with previously developed microsensors. The sensing area of the temperature microsensor is $350 \times 350\ \mu m^2$, the voltage microsensor's sensing area is $350 \times 350\ \mu m^2$, and the current microsensor's sensing area is $350 \times 350\ \mu m^2$. In addition to the voltage and current microsensors, the temperature microsensor utilizes a serpentine design to increase resistance, with a wire width of 50 μm and a serpentine wire width of 10 μm.

2.2 Fabrication of flexible three-in-one microsensor

MEMS technology has revolutionized the field of sensor and actuator fabrication.(31–38) By leveraging MEMS technology, microsensors and microactuators are now being produced with high precision and functionality. The fabrication of the flexible three-in-one microsensor developed in this study utilizes various micro-electromechanical process technologies multiple times, including physical vapor deposition (PVD), lithography, lift-off, and wet etching. The substrate is a 50-μm-thick polyimide (PI) film known for its excellent strength, stretchability, high-temperature resistance, and chemical resistance. Gold is used as the main electrode material, with titanium serving as the adhesive layer. Although wet etching processes are cost-effective, controlling the quality can be challenging in manually fabricated microsensors owing to difficulties in managing time parameters. Wet etching processes often lead to overetching, causing larger signal variations in each microsensor. To address this issue and achieve standardization, lift-off is adopted as the primary electrode fabrication process instead of wet etching, as it provides better control over the manufacturing parameters.

The process of fabricating the temperature, voltage, and current microsensors in this study is as follows:

(a) Polyimide film cleaning

First, it is essential to clean the PI film, as an insufficiently clean and smooth substrate surface can impact the stability of subsequent processes and may even lead to structural peeling or damage. As shown in Fig. 1(a), the polyimide film is sequentially immersed in organic solvents, namely, acetone and methanol, for cleaning. After ultrasonic washing for 3 min using an ultrasonic cleaning machine, the substrate is rinsed with deionized water to remove any remaining organic solvents from the surface. The substrate surface is then dried using a compressed air gun and placed on a heating plate for baking at 110 °C for 4 min.

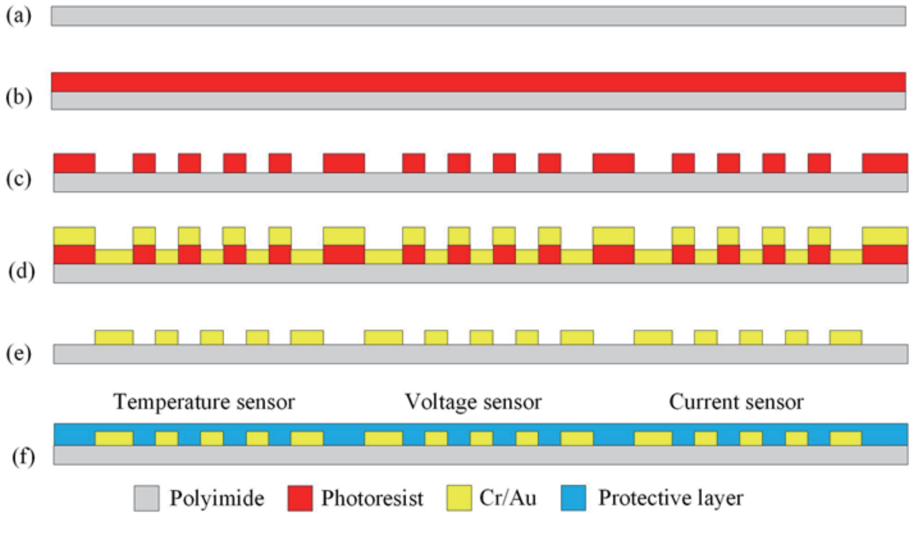

Fig. 1. (Color online) Fabrication flow of three-in-one microsensor: (a) cleaning PI substrate, (b) spinning photoresist, (c) photolithography, (d) depositing Cr/Au, (e) lift-off metal, and (f) depositing protective layer.

(b) Photoresist coating

As shown in Fig. 1(b), a spin coater is utilized to uniformly coat the sample with a positive photoresist (AZ® P4620).

(c) UV photolithography

The electrode layer photolithography is a crucial step in this manufacturing process, and any slight mishandling during the definition of patterns can significantly impact the performance of the final microsensor product. As shown in Fig. 1(c), the exposure process is initiated using a dual-sided alignment exposure machine. After the exposure, the development process begins. In this experiment, AZ® 400K is used as the developing solution.

(d) Metal deposition

As shown in Fig. 1(d), an electron beam evaporation system is used to deposit chromium and gold onto the PI layer. This falls within the realm of PVD, characterized by the advantage of dense film deposition and strong adhesion to the substrate. The principle of an electron beam evaporation machine involves using electron bombardment on a target material, raising its temperature to the melting point, causing it to evaporate and deposit onto the surface of the target object. Gold is chosen as the sensing material owing to its stable chemical properties, simple processing, high linearity, and low cost. Chromium is used as the adhesive layer.

(e) Metal lift-off process

Immediately after the deposition, the sample undergoes the lift-off process. As shown in Fig. 1(e), the lift-off process involves using acetone to remove the original photoresist, simultaneously lifting off the excess metal, leaving only the metal pattern of the electrodes on the sample.

(f) Protective layer

As shown in Fig. 1(f), Fujifilm Durimide® LTC 9320 is used for a second round of exposure and development to enhance mechanical strength and provide an insulating protective layer suitable for harsh chemical environments. After completion, the results are observed using an optical microscope (OM), as depicted in Fig. 2.

2.3 Flexible circuit board design for flexible three-in-one microsensor

In the past, microsensors using ceramic circuit boards faced challenges owing to the weight of the ceramic board and heavy wires. This weight could lead to bending when embedded inside batteries, causing the adhesive holding the microsensor to fail. Consequently, this bending could result in the detachment of conductive gels and silver paint, ultimately damaging the microsensor. Therefore, in this study, we innovatively developed a flexible printed circuit (FPC). The FPC design was created using drawing software (AUTOCAD), and mass production was outsourced to industry manufacturers. The FPC is integrated with the flexible three-in-one microsensor, addressing the aforementioned issues. This integration not only solves the bending problem but also allows for a reduction in the size of the microsensor design. In the past, a four-inch wafer could produce only five sets of microsensors, whereas now, it can produce 16 sets, significantly increasing output and reducing costs. The total length of the FPC is approximately 26 cm, utilizing PI as the base material. Apart from metal pads on the top and bottom, the rest of the

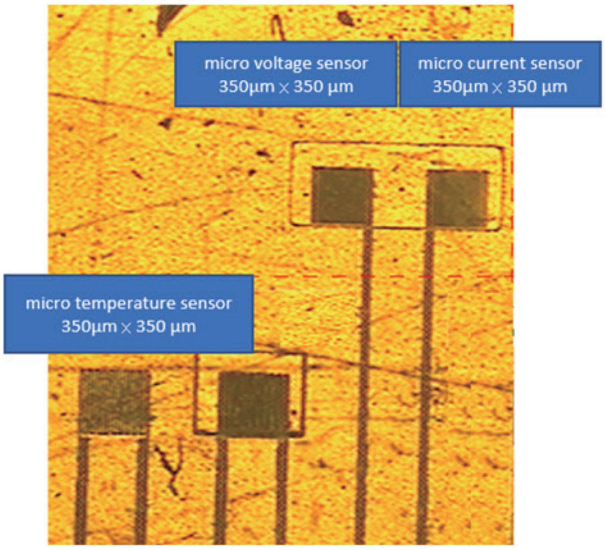

Fig. 2. (Color online) OM image of three-in-one microsensor.

circuits are covered and protected by a thin PI layer. Additionally, the bottom side is equipped with 0.3 mm gold fingers.

2.4 Flexible three-in-one microsensor integrated with flexible circuit board backend

The connection and integration between the flexible three-in-one microsensor and FPC involve the use of an anisotropic conductive film (ACF) for adhesion. The ACF exhibits the characteristics of vertical conductivity and horizontal insulation, excellent adhesion, high-temperature resistance, high-pressure resistance, and low thickness. Hence, it is chosen as the adhesive material. Before usage, it should be pressed at specified temperature and pressure simultaneously to establish conductivity. As conventional heat presses cannot be employed, a vendor with pulse heat press machines was sought. Pulse heat presses allow for instantaneous heating while applying pressure, achieving simultaneous bonding. After practical testing, the flexible three-in-one microsensor and FPC were successfully bonded and made conductive using the ACF. Subsequently, the gold finger part was connected to the FPC adapter board, completing the integration of the flexible three-in-one microsensor with the backend of the flexible circuit board.

The measurement circuit design of the three-in-one microsensor embedded in the PEMWE integrates temperature, voltage, and current sensing functions to provide the comprehensive environmental monitoring required during the operation of the water electrolyzer. The three-in-one microsensor provides an effective method to monitor the operating environment of PEMWE and helps optimize their performance and safety of PEMWE. At the same time, the design that integrates multiple sensing functions can also reduce the cost and complexity of the system and improve the feasibility and practicality of its application.

3. Circuit Design of Three-in-one Microsensor

In this study, the Arduino Mega 2560 is employed as the development board for data acquisition. Since Arduino measurements can only capture voltage values and cannot directly read current and resistance values, it is necessary to convert the current and resistance values into voltage signals for analysis.

3.1 Temperature microsensor measurement principle and circuit

The temperature microsensor utilized in this study is a resistance temperature detector (RTD) with a serpentine electrode structure. The principle is based on the work of Serway *et al.*,(39) which states that within a limited temperature range, for typical metal conductors, the resistance that changes roughly with temperature can be expressed as

$$R = R_0\left[1 + a\left(T - T_0\right)\right], \tag{1}$$

where R is the resistivity at a certain temperature (T), R_0 is the resistivity at a certain reference temperature (T_0, usually 20 °C), and α is the temperature coefficient of resistance.

A resistive temperature microsensor can use a voltage divider circuit (as shown in Fig. 3) to measure voltage variations, which can then be converted into resistance changes.

3.2 Voltage microsensor measurement principle and circuit

The circuit design for the voltage microsensor is illustrated in Fig. 4. It takes the form of a probe, and owing to the low resistivity of gold (2.44×10^{-8} Ω·m), the resistance generated by the gold-made wire is negligible. Therefore, the wire is directly connected to the Arduino Mega 2560 for the measurement of the internal voltage.

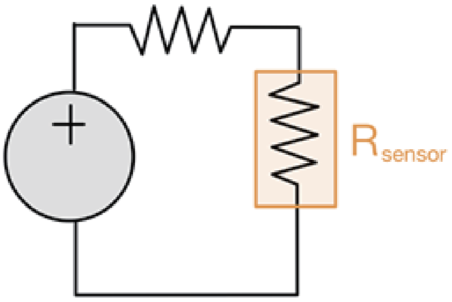

Fig. 3. (Color online) Voltage divider circuit for temperature microsensor.

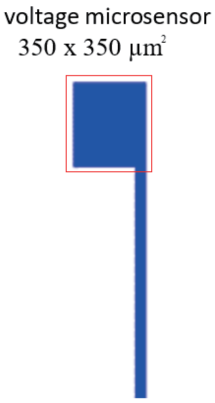

Fig. 4. (Color online) Circuit diagram of voltage microsensor.

3.3 Current microsensor measurement principle and circuit

The incoming current signal is amplified and converted into a voltage signal through a transimpedance amplifier circuit (as shown in Fig. 5). Both the current and voltage microsensors are in probe form and embedded in the water electrolyzer to capture local current signals. The circuit design is depicted in Fig. 6. The relationship between the output voltage and current microsensor values can be expressed as

$$V_{\mathrm{out}} = I_{\mathrm{sensor}} \times R. \tag{2}$$

3.4 Circuit integration of three-in-one microsensor

The circuits of the microsensors are integrated, and a schematic diagram is drawn. Subsequently, a printed circuit board (PCB) design is planned with each component illustrated (as depicted in Fig. 7). The design is then submitted to a manufacturer to produce the final product (as seen in Fig. 8).

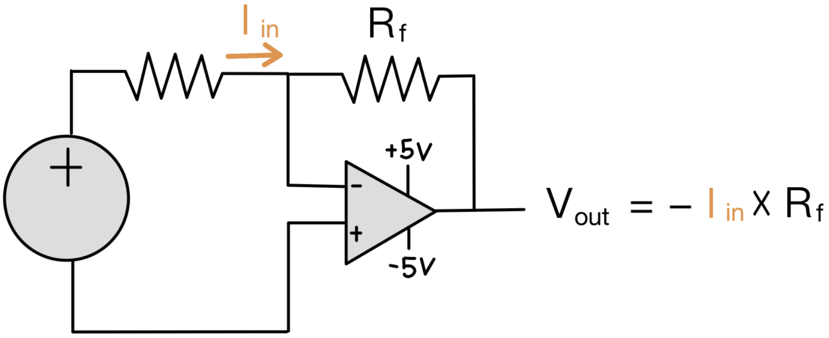

Fig. 5. (Color online) Circuit diagram of current microsensor.

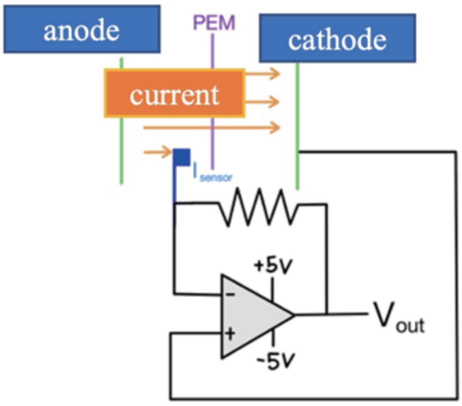

Fig. 6. (Color online) Circuit design of current microsensor.

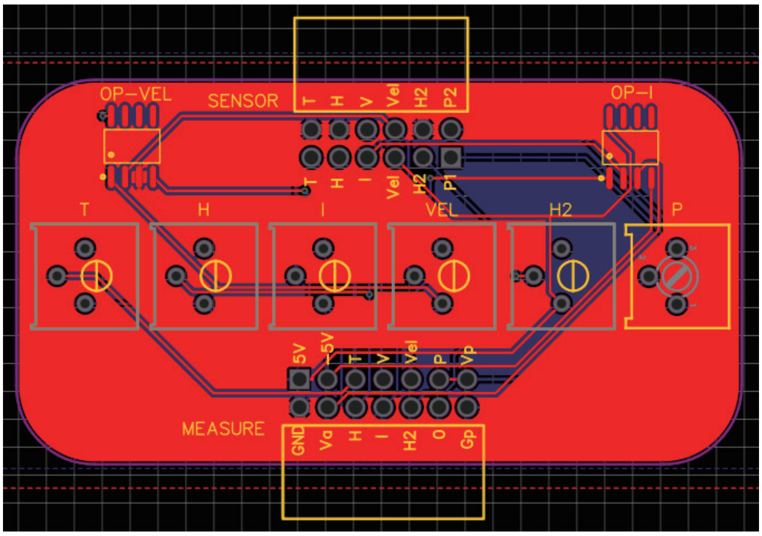

Fig. 7. (Color online) PCB design of three-in-one microsensor circuit.

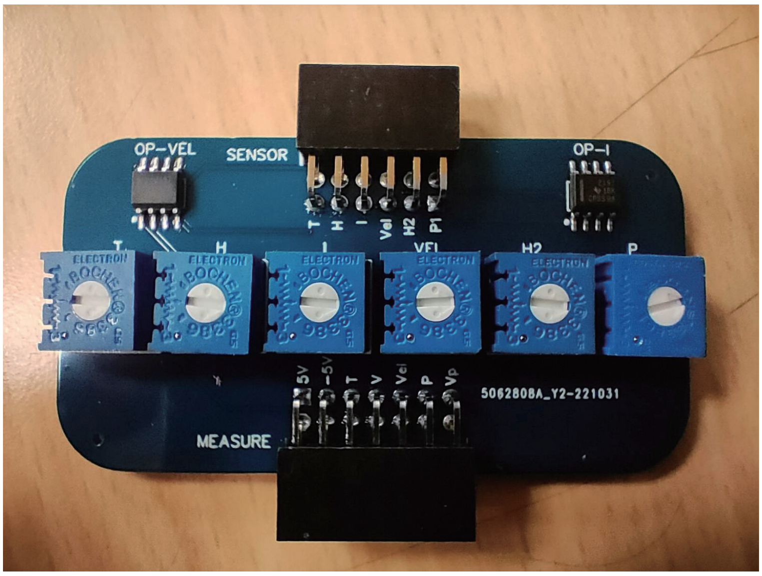

Fig. 8. (Color online) Physical image of PCB for three-in-one microsensor circuit.

4. Reading and Calibration of Three-in-one Microsensor

4.1 Real-time reading of three-in-one microsensor signals

The Arduino code for reading temperature, voltage, and current signals is written and every one hundred data points are averaged to mitigate noise.

4.2 Calibration of three-in-one microsensor

The temperature microsensor used in this study is a resistive temperature detector that requires calibration. The calibration curves for temperature exhibit a highly linear relationship, as shown in Fig. 9. Voltage and current are directly read without the need for calibration.

5. Real-time Microscopic Diagnosis of PEMWE

5.1 Embedding the three-in-one microsensor into PEMWE

The completed three-in-one microsensor is embedded into the PEMWE for real-time data monitoring and recording. The microsensor is inserted between the porous titanium plate layer and the catalyst, as illustrated in Fig. 10.

After embedding, the circuit device is connected, including amplifiers supplied with the positive and negative voltage signals required by the power supply. The converted voltage signals

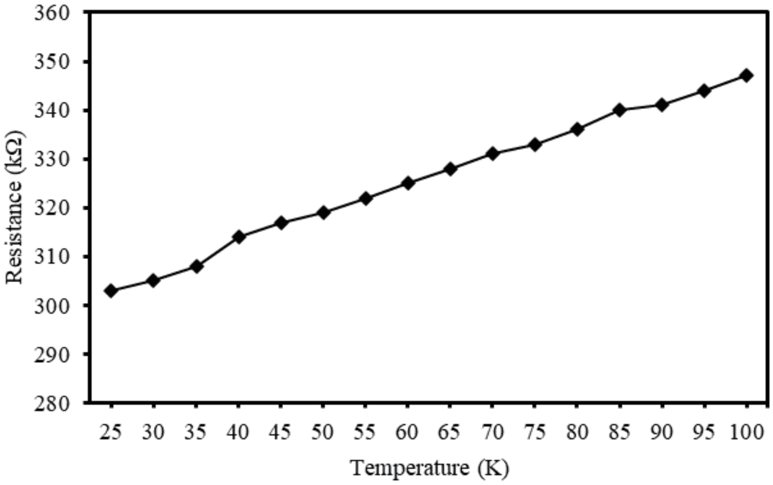

Fig. 9. Temperature calibration curve.

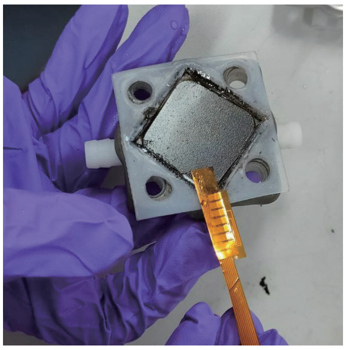

Fig. 10. (Color online) Embedding position of three-in-one microsensor.

are then input into the Arduino Mega 2560, and real-time data are captured from the computer. The setup is depicted in Fig. 11.

5.2 Local temperature and voltage distributions of PEMWE

Figure 12 shows the distributions of local temperature and voltage. It can be observed that the internal voltage varies linearly with the voltage supplied by the power supply, indicating accurate voltage measurement. However, the internal voltage is lower, suggesting that the ohmic impedance between the anode and the porous titanium plate consumes some voltage, leading to

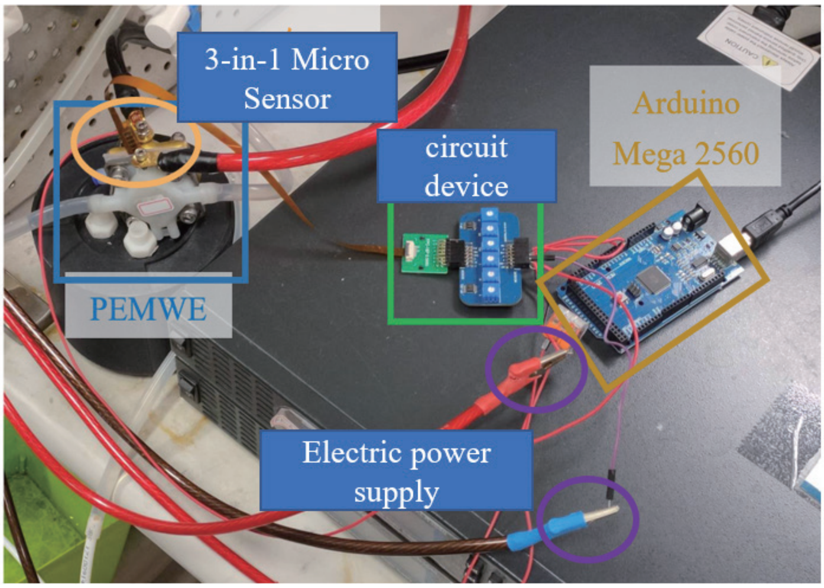

Fig. 11. (Color online) Circuit setup with three-in-one microsensor embedded in PEMWE.

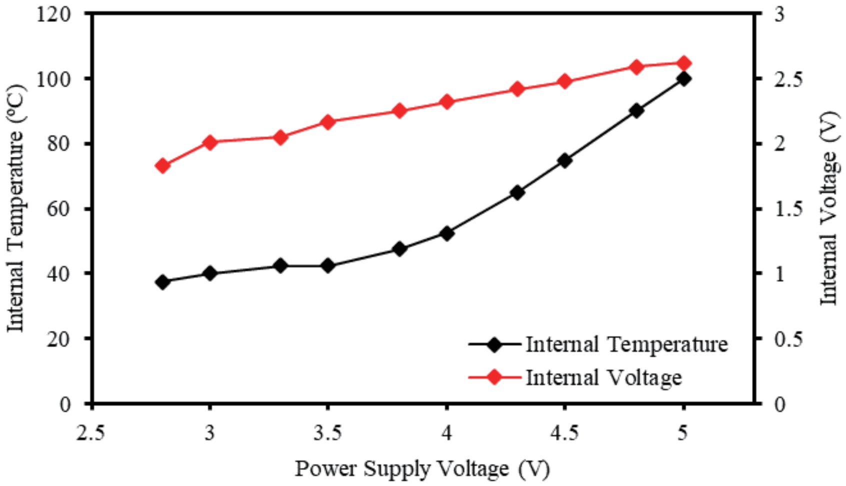

Fig. 12. (Color online) Local temperature and voltage distributions.

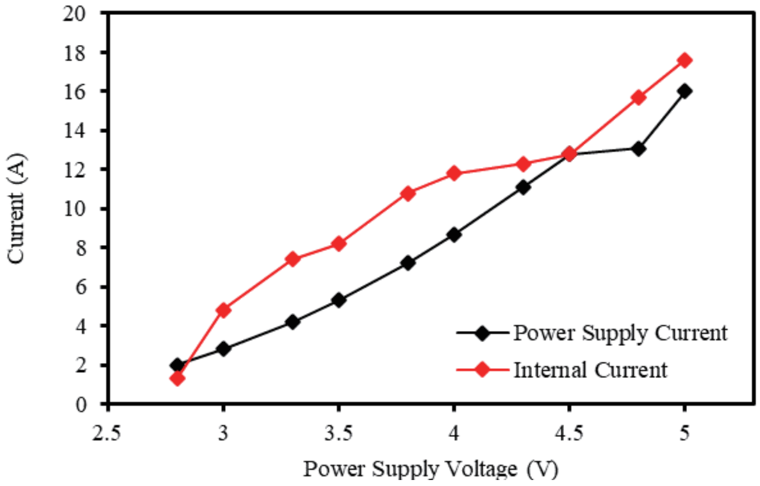

Fig. 13. (Color online) Local current distribution.

an increase in internal temperature. Additionally, the internal temperature and the voltage provided by the power supply exhibit a two-stage linear change. It is inferred that when the power supply provides 3.5–3.8 V, it surpasses the energy barrier of the PEMWE, causing a significant increase in current density and a more pronounced polarization effect.

5.3 Local current distribution of PEMWE

Figure 13 shows the distribution of local current. It can be observed that the internal current and the current provided by the power supply both show an increasing trend. However, the internal current variation is less stable, suggesting an uneven coating of the anode catalyst, leading to unstable performance reflected in the current data.

6. Conclusions

We successfully integrated the measurement circuit of a three-in-one microsensor, utilizing a PCB to create a modular system. The application of this system was demonstrated in real-time microscale diagnostics within a PEMWE. The primary objective was to facilitate the instantaneous extraction of data through the designed circuit, enabling computers to capture real-time information for future applications. The embedded three-in-one microsensor within the PEMWE provided authentic operational data concerning local temperature, voltage, and current. This real-time feedback allows the control system of the water electrolyzer to promptly adjust to optimal operating parameters, ultimately enhancing the performance and extending the lifespan of the PEMWE. The incorporation of this innovative circuit design not only allows for immediate data retrieval but also opens avenues for further developments and applications in the future.

Acknowledgments

The authors would like to thank the National Science and Technology Council of R.O.C. for its financial support through the grants MOST 109-2622-E-155-008, 110-2622-E-155-014, 110-2622-E-155-001, 111-2622-8-155-004-TM, and 112-2622-8-155-004-TM. The authors would like to thank the HOMY Technology, YZU Fuel Cell Center, and NENS Common Lab for providing access to their research facilities.

References

1 N. F. Asri, T. Husaini, A. Sulong, E. H. Majlan, and W. R. W. Daud: Int. J. Hydrogen Energy **42** (2017) 9135. https://doi.org/10.1016/j.ijhydene.2016.06.241
2 J. Y. Chen, D. Zhou, C. Lyu, and C. Lu: Int. J. Hydrogen Energy **42** (2017) 20230. https://doi.org/10.1016/j.ijhydene.2017.05.241
3 D. A. Langlois, A. S. Lee, N. Macauley, S. Maurya, M. E. Hawley, S. D. Yim, and Y. S. Kim: J. Power Sources **396** (2018) 345. https://doi.org/10.1016/j.jpowsour.2018.06.013
4 J. Jin, M. Hu, and X. Zhao: Int. J. Hydrogen Energy **45** (2020) 23310. https://doi.org/10.1016/j.ijhydene.2020.06.059
5 F.-C. Wang and W.-H. Fang: Int. J. Hydrogen Energy **42** (2017) 10376. https://doi.org/10.1016/j.ijhydene.2017.03.040
6 J. Han, Y. Kim, T. Kim, and S. Yu: Measurement **190** (2022) 110666. https://doi.org/10.1016/j.measurement.2021.110666
7 K. Handayani, P. Anugrah, F. Goembira, I. Overland, B. Suryadi, and A. Swandaru: Appl. Energy **311** (2022) 118580. https://doi.org/10.1016/j.apenergy.2022.118580
8 G. Wicks and J. Simon: Materials Innovations in an Emerging Hydrogen Economy (John Wiley & Sons, 2009).
9 K. Yue, J. Liu, Y. Zhu, C. Xia, P. Wang, J. Zhang, Y. Kong, X. Wang, Y. Yan, and B. Y. Xia: Energy Environ. Sci. **14** (2021) 6546. https://doi.org/10.1039/D1EE02606B
10 J. Q. Chi, X. J. Zeng, X. Shang, B. Dong, Y. M. Chai, C. G. Liu, M. Marin, and Y. Yin: Adv. Funct. Mater. **29** (2019) 1901790. https://doi.org/10.1002/adfm.201901790
11 W. Ji, K. Zhang, K. Zhan, P. Wang, X. Wang, and Y. Yan: Chin. J. Struct. Chem. **41** (2022) 2205015. https://doi.org/10.14102/j.cnki.0254-5861.2022-0106
12 G. Sang, P. Xu, T. Yan, V. Murugadoss, N. Naik, Y. Ding, and Z. Guo: Nano Micro Lett. **13** (2021) 1. https://doi.org/10.1007/s40820-021-00677-5
13 Y. Yan, J.-Y. Zhang, X.-R. Shi, Y. Zhu, C. Xia, S. Zaman, X. Hu, X. Wang, and B. Y. Xia: ACS Nano **15** (2021) 10286. https://doi.org/10.1021/acsnano.1c02440
14 H. You, Z. Zhuo, X. Lu, Y. Liu, Y. Guo, W. Wang, H. Yang, X. Wu, H. Li, and T. Zhai: CCS Chem. **1** (2019) 396. https://doi.org/10.31635/ccschem.019.20190022
15 Y. Chen, C. Liu, J. Xu, C. Xia, P. Wang, B. Y. Xia, Y. Yan, and X. Wang: Small Struct. **4** (2023) 2200130. https://doi.org/10.1002/sstr.202200130
16 P. Diéguez, A. Ursúa, P. Sanchis, C. Sopena, E. Guelbenzu, and L. Gandía: Int. J. Hydrogen Energy **33** (2008) 7338. https://doi.org/10.1016/j.ijhydene.2008.09.051
17 G. S. Ogumerem and E. N. Pistikopoulos: J. Process Control **91** (2020) 37. https://doi.org/10.1016/j.jprocont.2020.05.002
18 J. A. Turner: Science **305** (2004) 972. https://doi.org/10.1126/science.1103197
19 A. Ursua, L. M. Gandia, and P. Sanchis: Proc. IEEE **100** (2011) 410. https://doi.org/10.1109/JPROC.2011.2156750
20 F. Barbir: Sol. Energy **78** (2005) 661. https://doi.org/10.1016/j.solener.2004.09.003
21 K. Kavadias, D. Apostolou, and J. Kaldellis: Appl. Energy **227** (2018) 574. https://doi.org/10.1016/j.apenergy.2017.08.050
22 C. Ziogou, D. Ipsakis, P. Seferlis, S. Bezergianni, S. Papadopoulou, and S. Voutetakis: Energy **55** (2013) 58. https://doi.org/10.1016/j.energy.2013.03.017
23 M. Carmo, D. L. Fritz, J. Mergel, and D. Stolten: Int. J. Hydrog. Energy **38** (2013) 4901. https://doi.org/10.1016/j.ijhydene.2013.01.151
24 U. Babic, M. Suermann, F. N. Büchi, L. Gubler, and T. J. Schmidt: J. Electrochem. Soc. **164** (2017) F387. https://doi.org/10.1149/2.1441704jes

25 C.-Y. Lee, C.-H. Chen, Y.-H. Chien, and Z.-Y. Huang: Membranes **12** (2022) 779. https://doi.org/10.3390/membranes12080779

26 C.-Y. Lee, C.-H. Chen, S.-Y. Chen, and H.-T. Hsieh: Membranes **12** (2022) 919. https://doi.org/10.3390/membranes12100919

27 B. Jiang, H. Yuan, Q. Dang, T. Wang, T. Pang, Y. Cheng, K. Wu, X. Wu, and M. Shao: Int. J. Hydrogen Energy **44** (2019) 31121. https://doi.org/10.1016/j.ijhydene.2019.10.036

28 N. Lin and J. Zausch: Chem. Eng. Sci. **253** (2022) 117600. https://doi.org/10.1016/j.ces.2022.117600

29 M. Sartory, E. Wallnöfer-Ogris, P. Salman, T. Fellinger, M. Justl, A. Trattner, and M. Klell: Int. J. Hydrogen Energy **42** (2017) 30493. https://doi.org/10.1016/j.ijhydene.2017.10.112

30 C.-Y. Lee, C.-H. Chen, G.-B. Jung, S.-C. Li, and Y.-Z. Zeng: Micromachines **11** (2020) 1078. https://doi.org/10.3390/mi11121078

31 C.-C. Yeh, C.-L. Dai, and H.-F. Shih: Sens. Mater. **26** (2014) 75. https://doi.org/10.18494/SAM.2014.943

32 S. Kaminaga: Sens. Mater. **30** (2018) 723. https://doi.org/10.18494/SAM.2018.1814

33 C.-Y. Chen, M.-H. Li, and S.-S. Li: Sens. Mater. **30** (2018) 733. https://doi.org/10.18494/SAM.2018.1857

34 T. Takeshita, N. Makimoto, T. Kobayashi, and S. Takamatsu: Sens. Mater. **33** (2021) 1073. https://doi.org/10.18494/SAM.2021.2915

35 H. Honma, H. Mitsuya, G. Hashiguchi, H. Fujita, and H. Toshiyoshi: Sens. Mater. **34** (2022) 1527. https://doi.org/10.18494/SAM3785

36 Y.-C. Cheng, C.-L. Dai, C.-Y. Lee, P.-H. Chen, and P.-Z. Chang: Microsyst. Technol. **11** (2005) 444. https://doi.org/10.1007/s00542-004-0486-0

37 C.-L. Dai and J.-H. Chen: Microsyst. Technol. **12** (2006) 1143. https://doi.org/10.1007/s00542-006-0243-7

38 C.-L. Dai and W.-C. Yu: Microsyst. Technol. **12** (2006) 766. https://doi.org/10.1007/s00542-005-0077-8

39 R. A. Serway, J. W. Jewett, and V. Peroomian: Physics for Scientists and Engineers with Modern Physics 9th ed. (Brooks/Cole Cengage Learning, Australia, 2014).